For submission to Physics of Plasmas

Nonuniformity for rotated beam illumination in directly driven heavy-ion fusion

J. Runge* and B. G. Logan

Lawrence Berkeley National Laboratory and Virtual National Laboratory for Heavy Ion Fusion, Berkeley, CA 94720

(Dated: February 19, 2009)

Abstract

A key issue in heavy-ion beam inertial confinement fusion is target interaction, especially implosion symmetry. In this paper the 2D beam irradiation nonuniformity on the surface of a spherical target is studied. This is a first step to studies of 3D dynamical effects on target implosion. So far non-rotated beams have been studied. Because normal incidence may increase Rayleigh-Taylor instabilities, it has been suggested to rotate beams (to increase average uniformity) and hit the target tangentially. The level of beam irradiation uniformity, beam spill and normal incidence is calculated in this paper. In *Mathematica* the rotated beams are modelled as an annular integrated Gaussian beam. To simplify the chamber geometry, the illumination scheme is not a 4π system, but the beams are arranged on few polar rings around the target. The position of the beam spot rings is efficiently optimized using the analytical model. The number of rings and beams, rotation radii and widths are studied to optimize uniformity and spilled intensity. The results demonstrate that for a 60-beam system on four rings Peak-To-Valley nonuniformities of under 0.5% are possible.

*Electronic address: jakobrunge@gmail.com

I. INTRODUCTION

In inertial confinement fusion (ICF) heavy-ion beams (HIB) are used to generate a high energy density state [1–3]. A key issue is HIB-target interaction, especially implosion symmetry [4–6]. In this paper the beam irradiation nonuniformity on the surface of a spherical target is studied. This is a first step to studies of 3D dynamical e ects on target implosion. Beam nonuniformities have so far been studied in the case of non-rotated beams [7, 8]. Their normal incidence leads to a growth of Rayleigh-Taylor instabilities [9, 10] and it has therefore been suggested o setting the whole beam from its normal axis (the line running from final lens to nominal aiming point) by a displacement that is rotated rapidly about the axis. Then less intensity would hit the target normally and one could benefit from oblique/tangential incidence. Wobblers [3, 11, 12] can rotate ion beams with high frequency. The oscillatory e ect of the rotation is also assumed to mitigate the growth of instabilities [13].

Due to the high rotation frequency the ion beams in this paper are idealized as hollow beams, i.e. the rotation is integrated. In *Mathematica* [15] the rotated beams are modelled as a Gaussian beam with its center being rotated around a circle and the intensity averaged over the rotation. The circle radius is manipulated by the wobbler amplitude. The beams are arranged on polar rings around the target. The position of the beam spot rings is e ciently optimized to reduce nonuniformities using the analytical model. In various calculations the optimal number of rings and beams, their rotation radii and Gaussian widths are investigated.

In this examination the beam is modelled as a Gaussian distributed intensity, not as many incident ions. Therefore optimized uniformity refers to the irradiation uniformity on the target surface, not the volumetric energy deposition uniformity in the target layers caused by stopped ions. Optimizing the irradiation nonuniformity is believed to be an important first step. Further 3D studies that simulate incident ion particles and their energy deposition will have to take into account the shortening of deposition range for tangentially incident ions.

The paper is organized as follows. The first section will explain the simulation model and assumptions. The second section will give the calculation methods and numerical approximations. Then the results are presented and discussed.

II. SIMULATION MODEL

To simplify the chamber geometry, the beams are not equally distributed on 4π around the target, but rather on polar rings. This makes it easier to connect the accelerator to the target chamber. In a power plant the polar axis in Fig. 1 may be horizontal and the accelerated beams arrive from both sides with the beams bent towards the target. The beams are aimed radially so that the bending angle does not change once the target shrinks during the implosion. Then the rotation radius (wobbler amplitude) can be adjusted to the shrinking target (zooming). The intensity is calculated as the sum of rotated Gaussians from beam spots in Fig. 1 shown as cylinders for the case of four rings. The two rings near the poles have beam positions that are o set to the equatorial rings. This has been tested to reduce maximum deviations.

The rotated Gaussian beam is modelled as follows (Fig. 2). The center ($x_0 = a\cos\phi_0$ and $y_0 = a\sin\phi_0$ in polar coordinates) of a 2D Gaussian beam $e^{-\frac{(x-x_0)^2+(y-y_0)^2}{2s^2}}$ is integrated over a circle with radius a (wobbler rotation radius). The intensity E is given by:

$$E = \int_0^{2\pi} e^{-\frac{(x-a\cos(\phi_0))^2+(y-a\sin(\phi_0))^2}{2s^2}}\, d\phi_0 \tag{1}$$

where a is the rotation radius, s is the Gaussian width and x and y are cartesian coordinates with origin at the center around which the beam is rotated. Going over to polar coordinates $x = r\cos\phi$ and $y = r\sin\phi$ the integral becomes

$$E = e^{-\frac{a^2+r^2}{2s^2}} \int_0^{2\pi} e^{\frac{a\cdot r\cos(\phi+\phi_0)}{s^2}}\, d\phi_0 \tag{2}$$

$$= e^{-\frac{a^2+r^2}{2s^2}} \cdot 2\pi I_0\left(\frac{a\cdot r}{s^2}\right) \tag{3}$$

which yields the modified Bessel Function of the first kind of order zero with no ϕ-dependence [14].

This is the emitted beam intensity. To calculate the intensity deposition of one single rotated beam on the spherical target this intensity is multiplied by a Cosine factor cos(θ) to account for weaker intensity due to tangential incidence at the edges of the target. Furthermore a Heaviside-Theta function $(R\cos\theta)$ cuts o intensity beyond the target radius $R = 1$ and the rest will be spilled intensity. The resulting intensity on the target is then (without the unimportant prefactor):

$$E = e^{-\frac{a^2+r^2}{2s^2}} I_0\left(\frac{a\cdot r}{s^2}\right) \cdot \cos(\theta) \cdot \quad (R\cos\theta) \tag{4}$$

The coordinates used here are in the local coordinate system for every beam (Fig. 2). The coordinate r is to be understood as the radius in a tangential plane attached at the point where the center of the rotated beam hits the target. Whereas the coordinate θ is the polar angle from the spherical coordinate system of the target with θ = 0 being the point where the center of the rotated beam hits the target and $\theta = \frac{\pi}{2}$ the point where the beam hits the edge of the target sphere. In the calculation, for every beam the tangential plane is moved to the location of the center of the rotated beam, tangent to the target, and the intensity is then given as above in local coordinates. The total intensity is then given by the sum over all beams $E = E_{n,m}$, each with ring number m and beam number n.

$$E(\theta, \phi) = \sum_{m=1}^{N_{\text{rings}}} \sum_{n=1}^{N_{\text{beams}}} E_{n,m} \tag{5}$$

Now the new coordinates ($0 \leq \theta \leq \pi$, $0 \leq \phi \leq 2\pi$) are in the global spherical coordinate system of the target surface. N_{rings} is the number of rings and N_{beams} the number of beams on one ring.

The advantage of this rotated beam is its oblique incidence on the target. Fig. 3 compares the degree of normal incidence for a rotated and a non-rotated beam for a normalized deposition energy and the same percentage of spill. The intensity is shown in a polar plot with the beam coming from the top. The dotted beam represents a non-rotated Gaussian beam. The normal incidence for the rotated beam is significantly reduced. But a smaller beam width is necessary.

III. CALCULATION METHOD

In ICF the beam irradiation nonuniformity on the fuel target must be suppressed under a few percent in order to achieve a symmetric fuel pellet implosion. Here the rms and Peak-to-Valley (PTV) nonuniformity are employed. The latter is defined as follows:

$$\text{PTV} = \frac{E_{Max} - E_{Min}}{2\langle E \rangle} \tag{6}$$

where $\langle E \rangle$ is the mean intensity, calculated numerically in polar coordinates as the sum of all beams (cut o beyond the target radius R) divided by $4\pi R^2$.

The maximum and minimum value are calculated on a mesh using a 1 degree resolution. The rms nonuniformity is calculated using the *Mathematica* function *NIntegrate* with a multiperiodic strategy which gives optimal convergence for analytic periodic integrands when the integration interval is exactly one period. Furthermore the unspilled intensity is calculated as the quotient of $\int_0^R e^{-\frac{a^2+r^2}{2s^2}} I_0\left(\frac{ar}{s^2}\right)\, dr / \int_0^\infty e^{-\frac{a^2+r^2}{2s^2}} I_0\left(\frac{ar}{s^2}\right)\, dr$. The target radius is R = 1. The position of the beam spot rings (angles α and β in Fig. 1) is optimized using the *Mathematica* function *NMinimize*, minimizing the root of the deviations of the mean to the 6th power for just three points. This was found to be su cient when the points are carefully chosen.

Additionally the optimal parameter configurations are analyzed in modes s_n^m of Spherical Harmonics Y_n^m:

$$s_n^m = \int_0^{2\pi} \int_0^{\pi} E(\theta,\phi) Y_n^m(\theta,\phi) R^2 \sin\theta \, d\theta d\phi \tag{7}$$

Again, the integration is carried out using the *Mathematica* function *NIntegrate* with a multiperiodic strategy.

IV. RESULTS

At first, the question of how many rings and beams are necessary is addressed. Fig. 6 shows that a scheme with just two rings it not enough to provide low nonuniformities. Furthermore 10 beams (40 total) on four rings are not much di erent from 20 beams per ring or more rings. So 10 beams per ring on four rings seems to be enough. Obviously more than four rings reduce nonuniformities further, but four rings are enough to reduce the nonuniformity below 1%. The case studied further in this paper deals with 15 beams per ring (60 total). The optimized angles are very similar for the 40 and 60 beam scheme.

For two configurations (both 60 beams, $\{a$ = 0.51, s = 0.4$\}$ and $\{a$ = 0.55, s = 0.3$\}$) the intensity deposition on the target sphere is shown in Fig. 4 and Fig. 5. The nonuniformities are exaggerated five-fold and show smooth maxima and minima. For both cases a PTV nonuniformity of under 0.8% and a rms nonuniformity of under 1.2% are achieved.

Fig. 7 shows the PTV nonuniformities and Fig. 8 the rms nonuniformities for the 60 beam scheme for di erent rotation radii and beam widths. The spill mentioned in the legend increases almost linearly from rotation radius a = 0.4 to a = 0.6. The rotation radius shown

here varies between a = 0.4 –as there are no minima before and the normal incidence is too high– and a = 0.6 as then the spilled intensity reaches more than 25% even for small widths. For a width more than s = 0.4 the minimum appears at a radius with more than 20% waste which is undesirable. The aim is to use a big rotation radius as this reduces normal incidence and still keep the spilled intensity below about 20%.

The minima in rms and PTV nonuniformity occur at slighlty di erent radii, especially for larger widths. Table I lists the minima in PTV and rms for various widths and the optimized angles. The explanation for two minima occuring for smaller radii is the following (Fig. 9): Looking at a polar cut ($0 \leq \theta \leq \pi$) the first minimum appears when the radius is so that the crests of the four beams do not overlap much. The second minima appears when they overlap with the crest of one beam filling the "hole" in the center of the next beam. The absolute minimum in both PTV and rms were found for a width s = 0.34 and radius a = 0.45 (PTV= 0.3% and rms= 0.33%), but slighty greater nonuniformities are reached for a desireably bigger rotation radius for other widths.

For every set of beam parameters the angles of the beam spot rings were optimized for least deviation from the mean. Small deviations of about one degree from the ideal angle will double or more the nonuniformity.

For two cases (s = 0.4 and s = 0.3) and their optimal radius the energy deposition is analyzed in Spherical Harmonics. The energy deposition is almost azimuthal symmetric (as can be expected from a scheme with 15 beams in ϕ-direction, but only four rings; for 10 beams per ring the situation would be di erent), the deviations in ϕ-direction are only about a tenth of the deviations in θ-direction. Fig. 10 and Fig. 11 show the absolute amplitudes of modes for the two cases. Due to the symmetry about the equator the odd modes in n are zero. The o set of the polar to the equatorial ring leads to an e ective even number of beams in azimuthal direction causing the odd m-modes to vanish. The dominant (0,0) mode is normalized to 1. The $m \neq 0$ modes are orders of magnitude smaller due to the high symmetry. These high mode nonuniformities will smooth out due to radiation transport [3].

V. CONCLUSION

The aim of this paper was to study the irradiation nonuniformity for the case of rotated beams in HIF. The results give an overview of irradiation nonuniformities that finally

cause Rayleigh-Taylor instabilities. The calculated parameters are a guideline for further 3D implosion studies.

The results show that low nonuniformities are accessible using rotated beams for an economical four polar ring scheme with 40 - 60 beams. The nonuniformity depends on the beam width. For each width there exist one or more minima in nonuniformity when the rotation radius is changed. The bigger the radius the less normal incidence. For widths more than s = 0.5 in units of target radius (eg 1mm for a 4mm diameter target) the minimum has too much spill though and smaller widths are desireable.

The oscillatory e ect of a rotated beam is also believed to have a stabilizing e ect on RT growth [13].

Acknowledgments

The authors would like to thank the Heavy Ion Fusion research group at Berkeley, especially John Barnard and Alex Friedman for many fruitful discussions. This research was carried out while the corresponding author was a visitor at Lawrence Berkeley National Laboratory, where he was hosted by the LBNL Fusion Energy program which operates under the auspices of the U.S. DOE under Contract DE-AC02-05CH11231. This author would like to acknowledge the Fulbright Commission and German Academic Foundation (Studienstiftung des deutschen Volkes) for financial and idealistic support. Special thanks to Alex Castro and Alexander Radebach.

[1] B.G. Logan, F. Bieniosek, C. Celata, E. Henestroza, J. Kwan, E.P. Lee, M. Leitner, L. Prost, P. Roy, P.A. Seidl, S. Eylon, J.-L. Vay, W. Waldron, S. Yu, J. Barnard, D. Callahan, R. Cohen, A. Friedman, D. Grote, M. Kireeff Covo, W.R. Meier, A. Molvik, S. Lund, R. Davidson, P. Efthimion, E. Gilson, L. Grisham, I. Kaganovich, H. Qin, E. Startsev, D. Rose, D. Welch, C. Olson, R. Kishek, P. OShea and I. Haber, Nucl. Instr. and Meth. A **544**, Issues 1-2 (2005)

[2] L.R. Prost, P.A. Seidl, F.M. Bieniosek, C. M. Celata, A. Faltens, D. Baca, E. Henestroza, J. W. Kwan, M. Leitner, W. L. Waldron, R. Cohen, A. Friedman, D. Grote, S. M. Lund, A. W. Molvik, E. Morse, Phys. Rev. ST Accel. Beams **8** (2005) 020101.

[3] S. Kawata, K. Horioka, M. Murakami, J. Hasegawa, K. Takayama, H. Yoneda, K. Miyazawa, T. Someya, A.I. Ogoyski, M. Seino, T. Kikuchi, T. Kawamura, M. Ogawa, Nucl. Instr. and Meth. A **577** (2007)

[4] B.G. Logan, L.J. Perkins, J.J. Barnard, Phys. Plasmas **15**, 072701 (2008)

[5] J. Sasaki, T. Nakamura, Y. Uchida, T. Someya, K. Shimizu, M. Shitamura, T. Teramoto, A. B. Blagoev, S. Kawata , Jpn. J. Appl. Phys. **40**, 968 (2001)

[6] M. Murakami, Appl. Phys. Lett. **27**, 1587 (1995)

[7] T. Someya, A.I. Ogoyski, S. Kawata T. Sasaki, Phys. Rev. ST Accel. Beams **7**, 044701 (2004)

[8] K. Miyazawa, A.I. Ogoyski, S. Kawata, T. Someya, T. Kikuchi, Phys. Plas. **12**, 2005

[9] S. Atzeni and J. Meyer-ter-Vehn, *The Physics of Inertial Fusion* (Clarendon press, Oxford, 2004) Ch. 8, pp. 237 to 299

[10] H.J. Kull, Phys. Rep. **206**, 199 (1991)

[11] S. Kawata, T. Sato, T. Teramoto, E. Bandoh, Y. Masubichi, I. Takahashi, Laser Part. Beams **11** (1993) 757

[12] B. Sharkov, Nucl. Instrum. Methods Phys. Res. A **577**, 14 (2007)

[13] S. Kawata, Y. Iizuka, Y. Kodera, A.I. Ogoyski, T. Kikuchi, "Robust Fuel Target in heavy ion inertial fusion", to appear in Nucl. Instr. and Meth. A, (2008)

[14] Abramowitz and Stegun, Handbook of Mathematical Functions, Dover, New York, 1970

[15] Wolfram Research, Inc., *Mathematica*, Version **6.0**, Champaign, IL (2007)

TABLE I: Minima in PTV for various parameters; width and radius are in units of target radius; PTV, rms and spill are in %; α and β are in degrees.

Width s	Radius a	PTV	rms	Spill	α	β
0.30	0.42	1.1	1.38	4.45	78.7320	37.5489
	0.55	0.7	0.99	9.76	68.5505	43.1670
0.32	0.44	0.4	1.03	6.60	78.7280	37.5032
	0.56	0.6	0.79	12.35	69.2377	42.6234
0.34	0.45	0.3	0.33	8.70	79.2266	37.3975
	0.57	0.9	0.92	15.04	69.6181	42.3236
0.36	0.47	0.3	0.45	11.45	79.4527	37.3224
	0.58	1.2	1.11	17.77	70.1234	41.9323
0.38	0.49	0.5	0.73	14.42	79.7292	37.2332
	0.59	1.3	1.21	19.83	70.5238	41.6483
0.40	0.51	0.6	1.18	17.52	80.3463	37.0715
0.42	0.55	0.7	1.13	21.91	81.1061	36.8236
0.44	0.57	1.0	1.71	25.13	82.8523	36.4239

FIG. 1: Illumination scheme with four rings; the beam spots are arranged all around the polar rings.

FIG. 2: One beam with Gaussian profile is rotated with rotation radius a over the circle from ϕ = 0 to 2π; r and ϕ are local coordinates (for every beam) in the plane attached to the target surface; θ is a coordinate in the target system (with origin at the center of the target).

FIG. 3: Polar plot of beam intensity for rotated and non-rotated beams (a = 0, a Gaussian beam that hits the target normally), intensity is proportional to distance from origin at given angle θ; both beams are normalized and have the same spill; the arrows indicate the incidence of the beam; parameters are $\{s$ = 0.3, a = 0.55$\}$ for the rotated and s = 0.464 for the non-rotated beam.

FIG. 4: Intensity deposition on target sphere for a four ring scheme with 15 beam spots per ring and beam parameters s = 0.3 and a = 0.55, deviations of the mean are exaggerated 5-fold.

FIG. 5: Intensity deposition on target sphere for a four ring scheme with 15 beam spots per ring and beam parameters s = 0.4 and a = 0.51, deviations of the mean are exaggerated 5-fold.

FIG. 6: Peak-To-Valley deviation for various beam spot schemes. ”60 on 2” means just two rings with 30 beams per ring.

FIG. 7: Peak-To-Valley deviation for four di erent beam widths; the percentages in the legend are the spill for small and big radii.

FIG. 8: rms deviation for four di erent beam widths; the percentages in the legend are the spill for small and big radii.

FIG. 9: Explanation for the two minima occuring for a width of s = 0.3; the left figure shows the minimum at a smaller rotation radius a = 0.42, where the crests of the beams do not overlap much; the right figure shows the minimum for the bigger rotation radius a = 0.55 where the crest of one beam fills in the "hole" of the next beam.

FIG. 10: Mode analysis for the s = 0.3 and a = 0.55 case; the zeroth mode is 1 and not shown.

FIG. 11: Mode analysis for the s = 0.4 and a = 0.51 case; the zeroth mode is 1 and not shown.

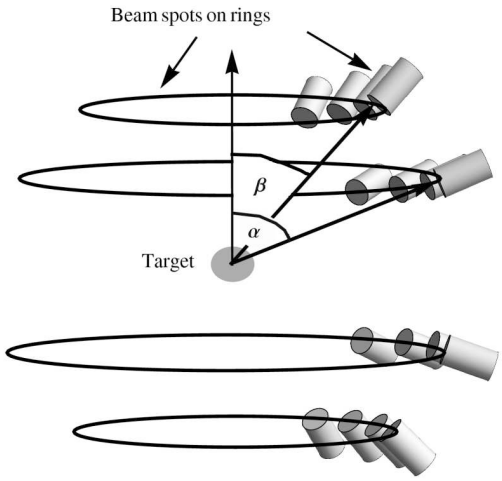

Figure 1

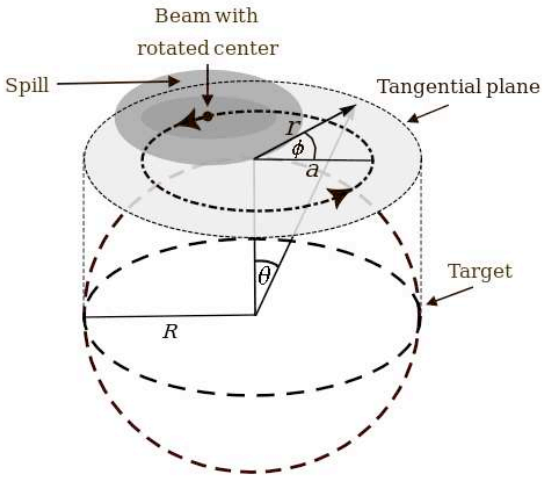

Figure 2

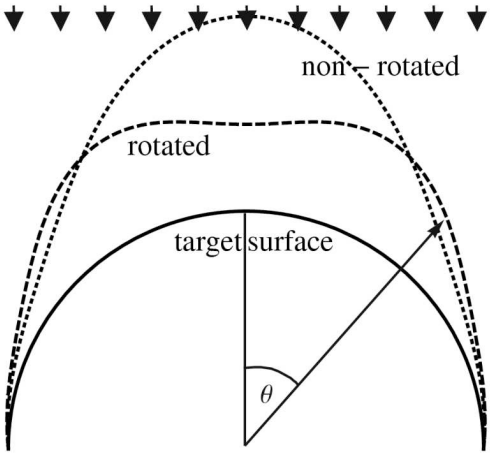

Figure 3

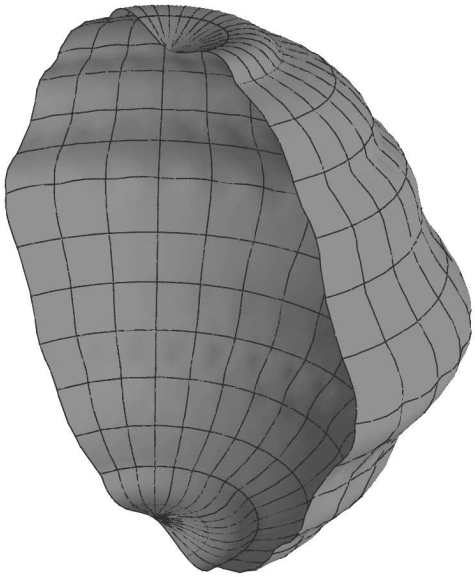

Figure 4

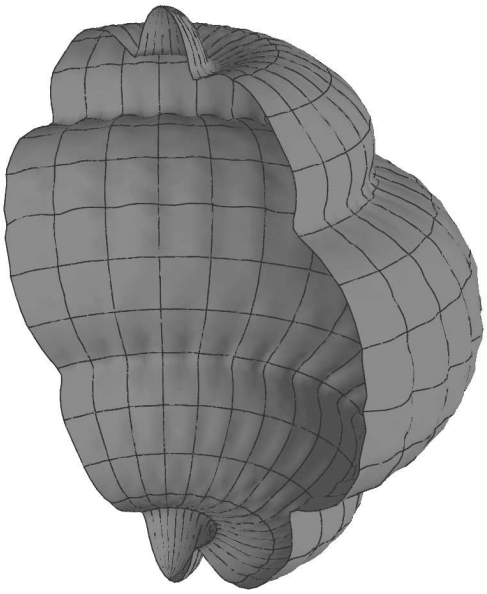

Figure 5

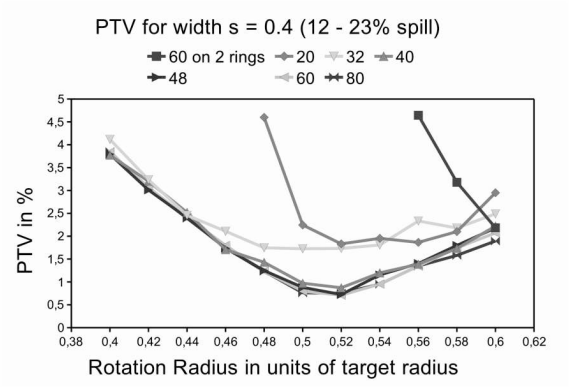

Figure 6

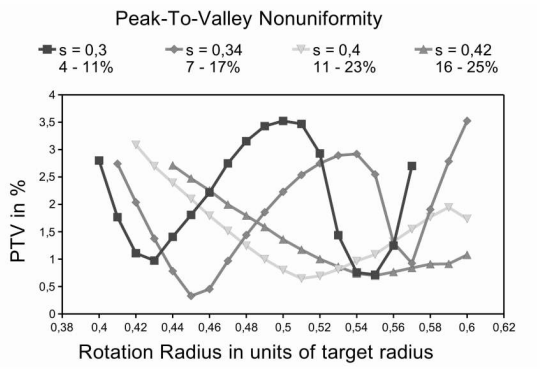

Figure 7

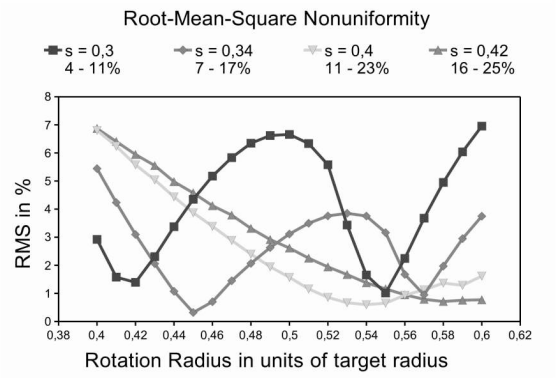

Figure 8

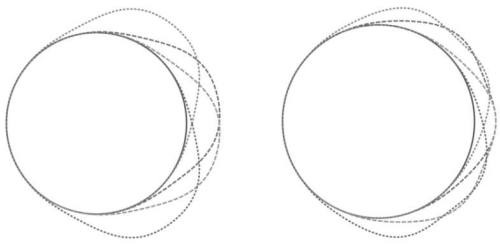

Figure 9

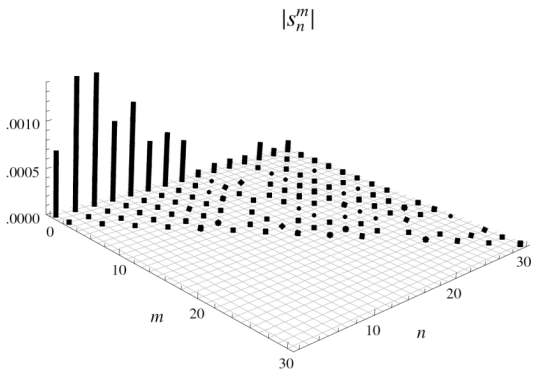

Figure 10

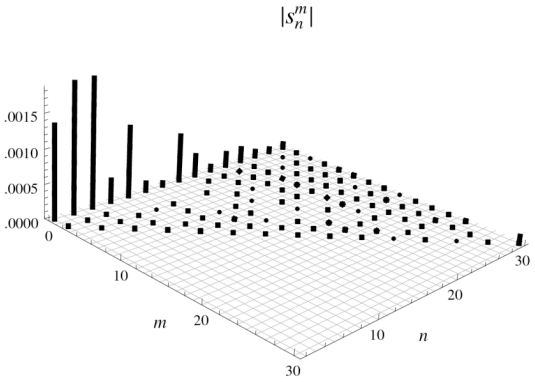

Figure 11